Resistive Power Loss Analysis of PV Modules Made From Halved 15.6 × 15.6 cm^2 Silicon PERC Solar Cells With Efficiencies up to 20.0%

Jens Müller, David Hinken, Susanne Blankemeyer, Heike Kohlenberg, Ulrike Sonntag, Karsten Bothe, Thorsten Dullweber, Marc Köntges, and Rolf Brendel

***Abstract*—In photovoltaic (PV) modules, the interconnection of solar cells is critical in terms of mechanical stability and resistive power losses. In this study, we analyze the interconnection of large-area 15.6 × 15.6 cm^2 industrial p-type passivated emitter and rear cell (PERC) solar cells in terms of resistive losses. For our analysis, we prepare a 3 × 3 minimodule from PERC solar cells with soldering pads and efficiencies up to 20.0%. We measure a significant cell-to-module (CTM) power loss of 8% at this module. For comparison, we prepare a 3 × 6 module consisting of halved 7.8 × 15.6 cm^2 PERC solar cells. Using a nanosecond laser to cut the finished solar cell in two pieces, no additional power loss is introduced by cutting. The CTM factor of 1.0 determined at the 3 × 6 module is explained using an analytical model describing the series resistance of the module interconnection. Using this model, we estimate for our current PERC cell generation and module process an output power of 275 W for 60 full-size cells and 285 W for 120 halved cells.**

***Index Terms*—Device simulation, module interconnection passivated emitter and rear cell (PERC) solar cells, resistive power loss.**

I. Introduction

THE RESISTIVE power loss in a photovoltaic (PV) module due to module interconnection

$$P_{\mathrm{loss,itc}} = I_{\mathrm{mpp}}^2 \times R_{\mathrm{s,itc}} \tag{1}$$

is the square of the current I_{mpp} at the maximum power point (MPP) and the series resistance $R_{\mathrm{s,itc}}$, which results from solar cell interconnection. As today's crystalline silicon cell technology offers electrical currents of more than $I_{\mathrm{mpp}} = 9$ A on 15.6 × 15.6 cm^2-sized wafers [1] a substantial resistive power loss P_{loss}, and therefore, a drop in *FF* is typically observed in PV modules [2]. Using ribbons with enlarged cross sections may reduce $R_{\mathrm{s,itc}}$. However, this either results in enhanced shadowing of active cell parts or induces mechanical stress during soldering and lamination [3]. More elegantly, P_{loss} is drastically reduced using halved solar cells as this halves the current *I*. However, this approach is used so far only by a few PV module manufacturers [4], [5].

We analyze the impact of resistive losses on 15.6 × 15.6 cm^2 p-type passivated emitter and rear cells (PERC); see, e.g., a review paper by Metz *et al.* [1]. For this purpose, we process PERC solar cells with soldering pads using production-type processing equipment at the ISFH Solar Technology Center (SolarTec). For the analysis of P_{loss}, we employ a simple-to-use analytic model that is both a simplification and extension of recently published models [6], [7]. We use an analytic approach rather than SPICE simulations as in [7] to allow for a quick and precise module optimization.

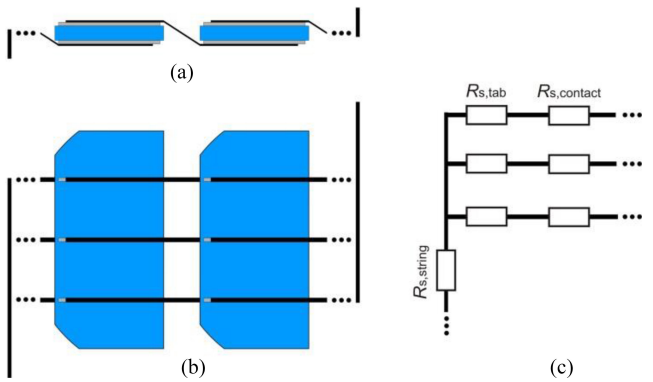

Fig. 1. (a) Side- and (b) top-view sketch of the cell interconnection used in this study. The cell interconnect ribbons connect the three busbars of the solar cell front with those on the rear of the adjacent cell. Strings of solar cells are interconnected by a string interconnect. (c) Equivalent circuit model of one string used to calculate the resistive power loss due to interconnection.

II. Resistive Power Loss

Within modules, the cell interconnection tab is soldered to the front and the rear side of a PERC solar cell. Thereby, it connects adjacent solar cells electrically. Strings of interconnected solar cells are then connected by string interconnects as it is schematically shown in Fig. 1. For the analysis of the series resistance

$$R_{\mathrm{s,itc}} = l \times \left(R_{\mathrm{s,string}} + \frac{m}{n} \left(R_{\mathrm{s,contact}} + R_{\mathrm{s,tab}} \right) \right) \tag{2}$$

Manuscript received July 7, 2014; revised September 9, 2014 and October 20, 2014; accepted October 29, 2014. Date of publication November 20, 2014; date of current version December 18, 2014. This work was supported by the German State of Lower Saxony and by the German Federal Ministry for Economic Affairs and Energy under Contract 0325641.

J. Müller, D. Hinken, S. Blankemeyer, H. Kohlenberg, U. Sonntag, K. Bothe, T. Dullweber, and M. Köntges are with the Institute for Solar Energy Research Hamelin, 31860 Emmerthal, Germany (e-mail: jensleinefelde@gmx.de; hinken@isfh.de; blankemeyer@isfh.de; kohlenberg@isfh.de; u.sonntag@isfh.de; bothe@isfh.de; dullweber@isfh.de; m.koentges@isfh.de).

R. Brendel is with the Institute for Solar Energy Research Hamelin, 31860 Emmerthal, Germany, and also with the Department of Solar Energy, Institute of Solid-State Physics, Leibniz University of Hanover, 30167 Hannover, Germany (e-mail: brendel@isfh.de).

Color versions of one or more of the figures in this paper are available online at http://ieeexplore.ieee.org.

Digital Object Identifier 10.1109/JPHOTOV.2014.2367868

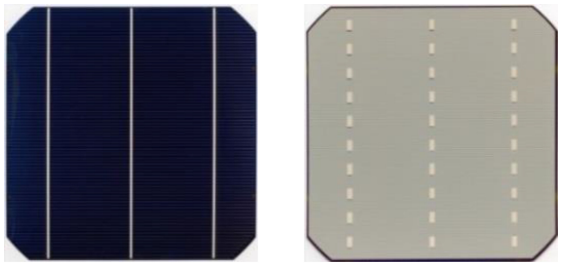

(a) (b)

Fig. 2. Images of 239-cm^2-sized pseudosquare PERC solar cells displaying (a) the front and (b) rear.

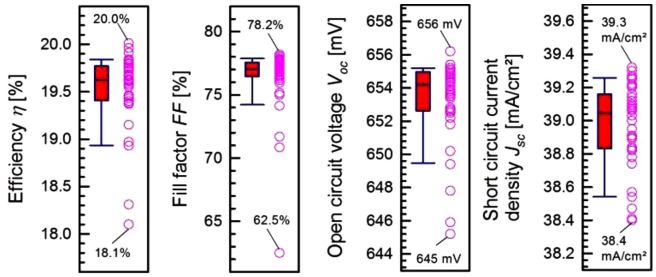

Fig. 3. Box-whisker plots, data distributions (pink circles), and min/max values of one 50-cell PERC batch. Bottom and top of the box mark the first and third quartile; the median is set by the line inside the box. Ends of the whiskers are located at one standard deviation above and below the mean of the data.

resulting from cell interconnection, we consider each contribution to the resistance: $R_{\mathrm{s,string}}$ the series resistances of the string interconnect; $R_{\mathrm{s,contact}}$ the contact resistance between tab and cell; and $R_{\mathrm{s,tab}}$ the resistance of the cell interconnect ribbons. In our calculation, we allow for arbitrary module configuration by considering a module with *l* cell strings, *m* cells per string, and *n* busbars per cell. In the case of halved solar cells, each solar cell piece adds to *m*. Together with (1), the analysis of $R_{\mathrm{s,itc}}$ allows us to calculate the resistive power loss for any module configuration. Note that this holds only as long as cell mismatch is negligible [8], which we proved for our case by SPICE simulations.

We calculate the string interconnect resistance

$$R_{\mathrm{s,string}} = \frac{\rho_{\mathrm{Cu}}}{A_{\mathrm{string}}} t_{\mathrm{string}} \tag{3}$$

from A_{string}, i.e., the cross-sectional area of the string interconnect, and its complete length t_{string}. String and cell interconnects are typically made from copper, which has an effective specific resistance $\rho_{\mathrm{Cu}} = 1.7\ \mu\Omega \cdot \mathrm{cm}$. To determine the effective cell interconnect resistance $R_{\mathrm{s,tab}}$, we consider the decrease in current along the interconnect as current is fed into or extracted from the solar cell, as described in [6]. An analysis of the cell interconnect power loss yields the effective cell interconnect ribbon resistance

$$R_{\mathrm{s,tab}} = \frac{\rho_{\mathrm{tab,eff}}}{A_{\mathrm{tab}}} \left(\frac{t_{\mathrm{tab}} - s}{3} + s \right) \tag{4}$$

where A_{tab} is the cross-sectional area of the cell interconnect, t_{tab} is the complete length of one cell interconnect ribbon from the front of one cell to the rear of the other, and *s* describes the length of cell interconnect ribbon that is not soldered to a solar cell in between cells. For interconnection of our PERC solar cells, we use a continuous solder connection. For this type of interconnection, Haedrich *et al.* [9] found that the contact resistance $R_{\mathrm{s,contact}}$ is negligibly small, and hence, it is neglected in the following analysis.

III. Solar Cell Process and Results

For our experiments, we fabricate industrial-type PERC solar cells with silver soldering pads for module interconnection, as shown in Fig. 2. The solar cells are processed on 15.6×15.6 cm^2 pseudosquare p-type Cz Si wafers of 180-μm thickness and a specific resistivity of 2–3 $\Omega \cdot$ cm.

The process flow is described in detail in [10]. Here, we just mention the most important steps. We use a dielectric protection layer to obtain a single-sided texture and phosphorus diffusion of the front side with a sheet resistance of 90 Ω/sq. Then, we remove phosphorus glass and protection layer by wet chemistry followed by deposition of an AlO_x/SiN_y rear passivation stack and front SiN_x antireflection coating. We locally ablate the rear passivation by laser in a line-shaped contact geometry. Subsequently, the silver front contact is formed by print-on-print screen printing with a finger width of around 60 μm. On the rear, we screen-print the silver pads followed by the rear aluminum contact, as shown in Fig. 2(a) and (b).

Most of our process steps above apply industrial-type pilot production equipment at the ISFH SolarTeC. With this process sequence, we reach a maximum output power of $P_{\mathrm{mpp}} = 4.78$ W delivered by an individual cell under standard test conditions (STC), which translates into a power conversion efficiency of $\eta = 20.0\%$ of the 239-cm^2-sized cell. The *I–V* parameters of a batch of 50 solar cells in Fig. 3 demonstrate the stability of our PERC process with narrow boxes and very few outliers, where 75% of the prepared solar cells have an efficiency higher than 19.5 %.

Rear passivation of silicon solar cells using dielectrics such as silicon oxide may lead to a strong injection dependence of the rear surface passivation [11]. Regarding solar cells under operation (i.e., within a solar module), such an injection dependence translates into a dependence of the solar cell efficiency on illumination intensity. The PERC solar cells in this study use an AlO_x/SiN_y rear passivation stack known to provide very small injection dependence [12]. We analyze the injection dependence of a 20.0% efficient (STC) PERC solar cell measuring the *I–V* characteristic at illumination levels between 0.1 and 1.0 sun. The resulting *I–V* curves are shown in Fig. 4. We observe only a very slight decrease in the short-circuit current density J_{sc} normalized by the illumination intensity P_{in} by 0.1 mA/cm^2/sun. This result confirms the small injection dependence of the rear passivation on our PERC solar cells. Furthermore, we compare the decrease in normalized efficiency from 1.0 to 0.1 sun of a 20% efficient (STC) PERC solar cell with a 19% efficient (STC) full-area back surface field (BSF) solar cell in Fig. 4. More details on the full-area BSF solar cell can be found in [13]. Whereas the normalized efficiency decreases by only 7%

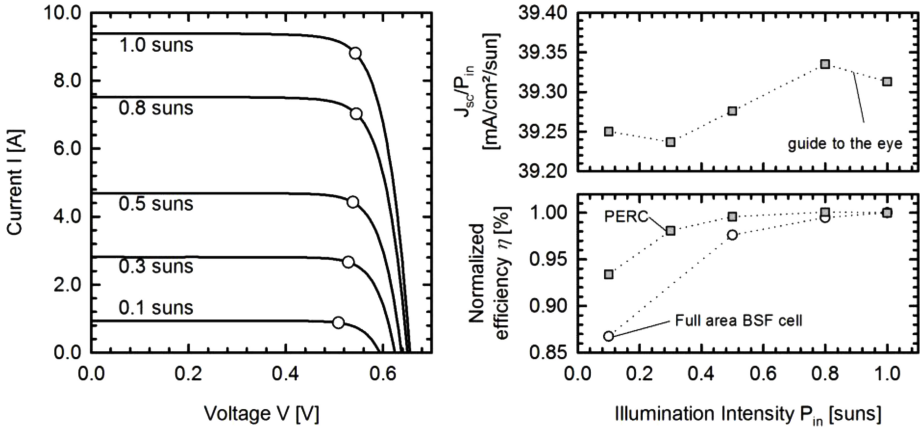

Fig. 4. *I–V* characteristics of a 20.0% efficient (STC) PERC solar cell measured at illumination levels between 1.0 and 0.1 sun (left). The short-circuit current density normalized by the illumination intensity $P_{\rm in}$ is approximately constant (upper right). The efficiency decreases from by 7%rel from 1.0 to 0.1 sun. For comparison, data from a 19% efficient (STC) solar cell with full-area BSF are demonstrated.

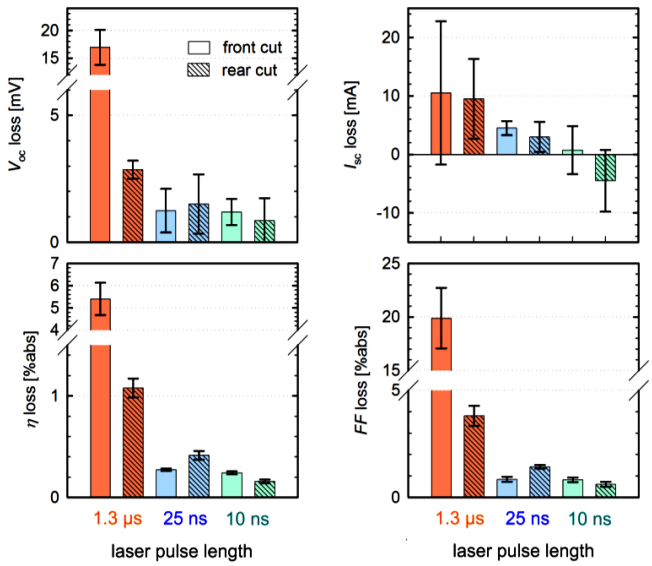

Fig. 5. Loss in PERC solar cell parameters (open-circuit voltage $V_{\rm oc}$, short-circuit current density $I_{\rm sc}$, efficiency η, fill factor *FF*) due to laser cut. Each bar represents four halved solar cells.

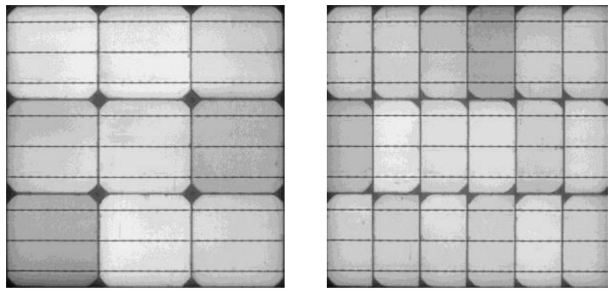

Fig. 6. EL picture of (a) 3 × 3 and (b) 3 × 6 module at low-current conditions ($I < 100$ mA). We used a cell-to-cell distance of 2 mm only.

relative for the PERC solar cell, the decrease is 13% relative in the case of the full-area BSF solar cell.

IV. Module Process

We evaluate the resistive power losses on modules with 3 × 3 full-sized and 3 × 6 halved PERC cells. In this analysis, we compare three laser systems used to cut the PERC solar cells. As laser treatment of silicon solar cells may introduce shunts and additional edge recombination [14], we measure the *I–V* curve under STC of the solar cells before and after laser cut. We compare laser systems with pulse lengths of 1.3 μs, 25 ns, and 10 ns and cut the solar cells from the front, as well as from the rear side. The impact of the cutting process is shown in Fig. 5. We measure the change in the *I–V* curve parameters before and after cutting, i.e., the loss in $V_{\rm oc}$ is calculated by the $V_{\rm oc}$ value before cutting minus the $V_{\rm oc}$ value after cutting. We find a very small decrease in the efficiency of 0.2 %abs when using a cut from the rear side with the 10-ns laser system [15]. The cell design, i.e., rear or front layout, has not been adopted for the laser cut.

For the solar cell interconnection, we use nonstructured cell interconnect ribbons. We interconnect the halved solar cells by facing the laser-cut side of one cell with the noncut side of the next cell to avoid shunting problems, as shown in Fig. 6(b). For both 3 × 3 and 3 × 6 modules, we use a cell-to-cell distance of 2 mm. At the end of each string, the 150-μm-thick and 1.5-mm-wide ribbons are connected by 200-μm-thick and 4-mm-wide string interconnects. The solar cell strings are then encapsulated, employing an UV transparent lamination EVA foil and a highly reflective backsheet. For the module front, we use a 52 × 52 cm^2 glass with antireflection coating on top. This leaves a 2.5-cm-wide inactive area around the solar cells for both modules. The EL images of both modules in Fig. 4 show the interconnection design. No cell cracks or disconnected cell parts are present.

V. Resistive Power Loss Analysis

The assessment of module power performance in terms of module efficiency depends critically on module size and, therefore, the area of inactive module parts such as the area in-between cells and between cells and the module frame [6].

TABLE I
COMPARISON OF THE 3 × 3 AND 3 × 6 MODULE *I–V* PARAMETERS WITH THOSE OF THE INDIVIDUAL SOLAR CELLS BEFORE INTERCONNECTION

	P_{mpp} [W]	*FF* [%]	V_{oc} [V]	I_{sc} [A]
9 PERC	42.4 $^{\Sigma}$	77.1 $^{\varnothing}$	5.89 $^{\Sigma}$	9.34 $^{\varnothing}$
3 × 3 Module	39.0	71.5	5.86	9.31
CTM-factor	0.92	0.93	0.995	0.997
18 halved PERC	42.5 $^{\Sigma}$	76.6 $^{\varnothing}$	11.77 $^{\Sigma}$	4.71 $^{\varnothing}$
3 × 6 Module	42.4	75.3	11.74	4.80
CTM-factor	1.00	0.98	1.00	1.02

Abbreviations used: ø - mean value Σ - sum of all cells.
The CTM factor is clearly dominated by a significant drop in FF for the 3 × 3 module made from full-area PERC cells.

TABLE II
COMPARISON OF MEASURED AND CALCULATED *I–V* PARAMETERS OF THE 3 × 3 AND 3 × 6 MODULES

	Interconnect thickness [μm]	P_{mpp} [W]	*FF* [%]
3 × 3 Module	150	39.0	71.5
Simulation	150	39.4	71.8
	200	39.9	72.7
3 × 6 Module	150	42.4	75.3
Simulation	150	42.6	75.5
	200	42.8	75.7

The simulation results are obtained from (6).
We analyze here the impact of the interconnector thickness. The modules were made using 1.5-mm-wide and 150-μm-thick interconnects.

Therefore, we analyze the cell-to-module (CTM) factor

$$\mathrm{CTM} = \frac{P_{\mathrm{mpp,module}}}{\sum P_{\mathrm{mpp,cells}}} \tag{5}$$

to assess our modules in terms of the resistive power loss. The CTM factor is also less dependent on the actual module size, allowing for a comparison of our minimodules to commercial 60-cell modules.

The maximum output power P_{mpp} of the two modules and of the PERC cells before interconnection is compared in Table I, together with other *I–V* parameters. The open-circuit voltage V_{oc} is doubled from full-area to halved PERC solar cells. This result is due to the doubled number of series-connected solar cells in the module. It demonstrates that the laser-cutting process does not introduce additional recombination. Comparing the 3 × 3 module and 3 × 6 module in short-circuit current density, we observe a small gain of 2%, which we attribute to the additional number of cell gaps in the case of the module made from halved solar cells. However, in the case of the 3 × 3 module, we measure a severe drop in *FF* of almost 8%, which leads to a rather low CTM factor of 0.92. This effect is less pronounced for the 3 × 6 module with a CTM factor of 1.00 because for this module, the current is halved, and thus, the power loss reduced [see (1)].

We calculate *FF* and $P_{\mathrm{mpp}} = I_{\mathrm{mpp}} \times V_{\mathrm{mpp}}$ of each module to prove this explanation quantitatively. For this purpose, we consider the drop in module voltage at MPP

$$V_{\mathrm{mpp,module}} = V_{\mathrm{mpp,cell}} - I_{\mathrm{mpp,cell}} \times R_{\mathrm{s,itc}} \tag{6}$$

compared with the average cell voltage $V_{\mathrm{mpp,cell}}$ at MPP, which is caused by the additional series resistance $R_{\mathrm{s,itc}}$ of the module interconnection. Equation (6) is then used to calculate module *FF* and P_{mpp}. Note that the maximum output current I_{mpp} may alter due to the voltage drop in (6), which is neglected here. Comparing SPICE simulations and our analytic calculations, we found that this leads to an overestimation in *FF* of less than $0.2\%_{\mathrm{abs}}$.

The comparison of actual and calculated module *FF* and P_{mpp} in Table II confirms our model in (2). For a more detailed analysis of the severe drop in FF for the module made from full-area solar cells, we compare in our calculation in Table II two different interconnect thicknesses: 150 and 200 μm. The actual modules were made from 150-μm-thick interconnects. Choosing the interconnect thickness is a tradeoff between mechanical stability, resistive power loss, as well as cost. While a thicker interconnect ribbon increases the material cost and the mechanical stress on the cells, a thinner ribbon will increase the resistive power loss. Therefore, the optimum ribbon thickness depends strongly on the actual module design and cost of the manufacturing process. From the simulation results in Table II, it can be seen that by increasing the interconnect thickness from 150 to 200 μm, the module output power P_{mpp} increases by 0.5 W. However, in the case of a module made from halved PERC solar cells, the increase in P_{mpp} is 0.2 W only.

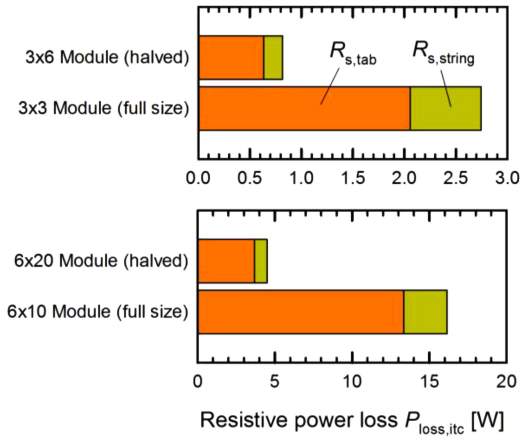

Fig. 7. Contribution of each series resistance contribution in (1) to the resistive power loss in (2) calculated for a 3 × 3, 3 × 6, 6 × 10, and 6 × 20 module. The contribution of contact resistance is neglected.

A calculation of the resistive power loss allows us to determine the impact of each interconnect series resistance. As an example, we compare in Fig. 7 the impact of $R_{\mathrm{s,tab}}$ and $R_{\mathrm{s,string}}$ on the resistive power loss for 3 × 3 module and 3 × 6 minimodules, as well as industrial size 6 × 10 module and 6 × 20 modules. We calculate the resistance of an individual interconnect ribbon to $R_{\mathrm{s,tab}} = 9.1$ mΩ for full-area PERC solar cells and 5.3 mΩ for halved solar cells. The string interconnect resistance is $R_{\mathrm{s,string}} = 7.6$ mΩ. For the analyzed examples in Fig. 7, the resistive power loss is dominated by $R_{\mathrm{s,tab}}$, accounting for 70–80% of the resistive power losses due to interconnection. In our simulations, we calculate a difference in the resistive power loss of 3 W for our minimodules made from full-area and halved PERC solar cells. For a commercial size module, we calculate a 10-W difference in the resistive power loss of modules made

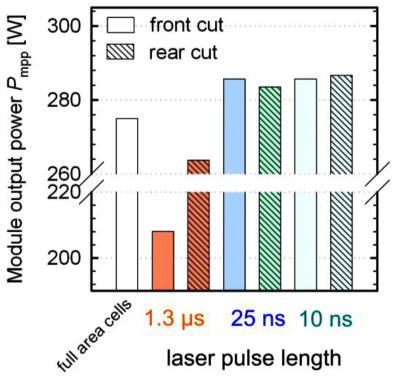

Fig. 8. Comparison of module output power P_{mpp} for modules made from 60 full-area and 120 halved PERC solar cells cut using the laser processes described in Section IV.

from full-area and halved PERC solar cells. Note that a potential gain in short-circuit current due to an increase in the number of cell gaps is neglected here.

To estimate the potential of our current PERC and module technology, we calculate P_{mpp} of large-size modules using (2) and (6). For this purpose, we compare the different laser processes used for the cut of solar cells, as presented in Section IV in Fig. 8. The lowest module output power $P_{\mathrm{mpp}} = 208$ W is expected in this comparison for the microsecond laser applied to the solar cell front side. For both nanosecond laser systems, we calculate almost equal module power output with a maximum difference in P_{mpp} of 1.1%. We predict from our model a maximum in $P_{\mathrm{mpp}} = 285$ W for a 6×20 module made using the 10-ns laser system applied to the solar cell rear. In comparison, we estimate for a 6×10 module from full-size PERC solar cells $P_{\mathrm{mpp}} = 275$ W.

VI. Conclusion

The presented analytic model of the resistive power loss in PV modules describes the series resistance due to the interconnection of PERC solar cells. We demonstrate large-area 15.6×15.6 cm^2 and 20.0% efficient solderable PERC solar cells. An analysis of the illumination dependence shows the low injection dependence of the applied AlO_x/SiN_y rear passivation stack with a decrease in short-circuit current density of 0.1 mA/cm^2 only comparing illumination at 0.1 and 1.0 sun. A minimodule prepared from 3×3 full-area PERC solar cells shows a significant CTM power loss of 8%. Using a laser cut from the rear side with a 10-ns laser system, we prepare halved PERC solar cells with a loss in efficiency as low as 0.2%abs. We observe a CTM factor of 1.0 for the 3×6 module made from halved PERC solar cells. Using our analytical model of the resistive power loss, we explain the significant difference in *FF* of the 3×3 and 3×6 minimodule. Using this model, we estimate, for our current PERC and module technology, an output power of 275 W using 60 full-size cells and 285 W for 120 halved cells.

Acknowledgment

The authors would like to thank the Institute for Solar Energy Research Hamelin (ISFH) laser team for their help with cutting solar cells and the ISFH characterization group for their help with measurements.

References

[1] A. Metz *et al.*," Industrial high performance crystalline silicon solar cells and modules based on rear surface passivation technology," *Solar Energy Mater. Solar Cells*, vol. 120, part A, pp. 417–425, 2013.
[2] F. Kiefer *et al.*, "Influence of solder pads to perc solar cells for module integration," *Energy Procedia*, vol. 38, pp. 368–374, 2013.
[3] S. Roberts *et al.*, "The reduction of module power losses by optimization of the tabbing ribbon," in *Proc. Eur. Photovoltaic Sol. Energy Conf.*, 2000, pp. 2378–2382.
[4] [Online]. Available: http://www.mitsubishielectric.com/bu/solar/pv_modules/monocrystalline/technologies.html
[5] J. H. Cunningham *et al.*, "Reaching grid parity using bp solar crystalline silicon technology," *Proc. 35th IEEE Photovoltaic Spec. Conf.*, Honolulu, HI, USA, 2010, pp. 1197–1202.
[6] I. Haedrich *et al.*, "PV module efficiency analysis and optimization," presented at the PV Rollout Conf., Boston, MA, USA, 2011.
[7] S. Guo *et al.*, "A quantitative analysis of photovoltaic modules using halved cells," *Int. J. Photoenergy*, vol. 2013, p. 739374, 2013.
[8] U. Yusufoglu *et al.*, "Simulation and analysis of PV module performance by innovative sorting methods," *Energy Procedia*, vol. 27, pp. 685–690, 2012.
[9] I. Haedrich *et al.*, "Minimizing the optical cell-to-module losses for MWT modules," *Energy Procedia*, vol. 38, pp. 355–361, 2012.
[10] T. Dullweber *et al.*, "Towards 20% efficient large-area screen-printed rear-passivated silicon solar cells," *Prog. Photovoltaic Res. Appl.*, vol. 20, pp. 630–638, 2012.
[11] A. Aberle *et al.*, "Impact of illumination level and oxide parameters on Shockley–Read–Hall recombination at the Si-SiO_2 interface," *J. Appl. Phys.*, vol. 71, pp. 4422–4431, 1992.
[12] B. Vermang *et al.*, "Assessment of the illumination dependency of Al_2O_3 and SiO_2 rear-passivated p-type silicon solar cells," *Phys. Status Solidi, Rapid Res. Lett.*, vol. 6, no. 6, pp. 259–261, 2012.
[13] H. Hannebauer *et al.*, "18.9%-efficient screen-printed solar cells applying a print-on-print process," in *Proc. 26th Eur. Photovoltaic Sol. Energy Conf.*, 2011, pp. 1607–1610.
[14] A. Hauser *et al.*, "Comparison of different techniques for edge isolation," presented at the 17th Eur. Photovoltaic Sol. Energy Conf., Munich, Germany, 2001.
[15] S. Eidelloth *et al.*, "High speed laser structuring of crystalline silicon solar cells," in *Proc. IEEE 34th Photovoltaic Spec. Conf.*, San Diego, CA, USA, 2009, pp. 2389–2394

Jens Müller received the Diploma degree in physics from the Georg-August-University Göttingen, Göttingen, Germany, in 2008 and the Ph.D. degree in the characterization of local aluminum alloyed contacts to silicon solar cells from the University of Hannover, Hannover, Germany, in 2013.

He joined the photovoltaic (PV) characterization group with the Institute for Solar Energy Research Hamelin, Emmerthal, Germany, in 2009. He is currently working on passivated emitter and rear cell solar cell development for PV module interconnection. His research interests include the characterization, modeling, and process development of crystalline silicon solar cells, as well as PV modules.

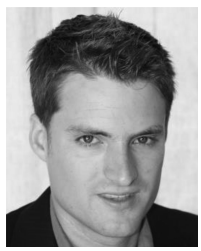

David Hinken studied physics with the University of Hanover, Hannover, Germany, and the University of La Laguna, Santa Cruz de Tenerife, Spain. He received the Physics Diploma degree in 2007 and the Ph.D. degree in physics in 2012, both from the University of Hanover, for his work on luminescence-based characterization of crystalline silicon solar cells.

He is currently with the Institute for Solar Energy Research Hamelin, Emmerthal, Germany, where he forms part of the solar cell characterization group and the PERC-to-module team, which develops improved module technology for PERC solar cells. His research interest focuses on the characterization, high precision measurement, the modeling of solar cells, and solar modules.

Susanne Blankemeyer was with Krane-Optik, Rheda-Wiedenbrück, Germany, until 1986, where she was trained as an optician. From 1999 to 2007, she was a Laboratory Assistant with the R&D Department of Orbotech: a manufacturer of automated optical inspection systems in Bad Pyrmont, Germany. In 2007, she joined the Module and Interconnection Technology Group, Institute for Solar Energy Research Hamelin, Emmerthal, Germany. She is currently involved in the development of novel interconnection techniques and the optimization of module concepts.

Heike Kohlenberg was with Kleinwanzlebener Saatzucht AG (KWS), Einbeck, Germany, where she completed her training as an agricultural-technical assistant in 1991. After that, she was responsible for quality control with Rigips SAINT-GOBAIN, Bodenwerder, Germany. In 2008, she joined the Institute for Solar Energy Research Hamelin, Emmerthal, Germany, where she prepared ion-implanted back-contact solar cells on n-type silicon subtrates with the silicon wafer solar cell group. She is currently responsible for the development of passivated emitter and rear cell solar cells for interconnection in photovoltaic modules.

Ulrike Sonntag was with Riedel-de Haen AG, Seelze, Germany, until 1993, where she was trained as a Chemical Laboratory Assistant and worked with the Quality Control group. From 1993 to 1997, she was with the Philipps-University Marburg, Germany, as a Laboratory Assistant with the Department of Biology and the Department of Chemistry. In 1998, she joined the silicon wafer solar cell group with the Institute for Solar Energy Research Hamelin, Emmerthal, Germany. She is currently involved in the process development of highly efficient passivated emitter and rear cell solar cells for interconnection in photovoltaic modules.

Karsten Bothe received the Physics Diploma degree in photoluminescence characterization of $Cu(InGa)Se_2$ with submicrometer resolution from the University of Oldenburg in 2001. Afterward, he joined the Institute for Solar Energy Research Hamelin (ISFH), Emmerthal, Germany, and received the Ph.D. degree on oxygen-related trapping and recombination centers in boron-doped crystalline silicon from the University of Hannover, Hannover, Germany, in 2006.

He studied physics with the Technische Universität Braunschweig, Braunschweig, Germany; the University of Sussex, Brighton, U.K.; and the University of Oldenburg, Oldenburg, Germany.

He then worked with the Nara Institute of Science and Technology, Japan, as a Research Fellow of the Germany Physical Society (DPG) and the German Research Association (DFG) on luminescence imaging. Since 2007, he has been the Head of the solar cell characterization group with the Institute for Solar Energy Research Hamelin. His current research interest is focused on the development of combined algorithms and measurement techniques for a quantitative local loss analysis of crystalline silicon solar cells. He works on camera-based luminescence imaging techniques for the characterization of silicon wafers and solar cells and studies the impact of defects on the solar cell performance in mono- and multicrystralline silicon. He has published more than 100 scientific papers in leading journals and conferences.

Thorsten Dullweber received the Ph.D. degree from the University of Stuttgart, Stuttgart, Germany, in 2002.

From 2001 to 2009, he was a Microelectronics Project Leader with Siemens, Infineon, and Qimonda. Since 2009, he has been leading the R&D group "solar cell production processes," Institute for Solar Energy Research Hamelin, Emmerthal, Germany, focusing on process and efficiency improvements of industrial-type screen-printed silicon solar cells.

Marc Köntges received the Ph.D. degree in physics on characterization of $CuInGaSe_2$ and CdTe thin-film solar cells from the University of Oldenburg, Oldenburg, Germany, in 2002.

Since 2002, he has been leading the thin-film technology group with the Institute for Solar Energy Research Hamelin (ISFH), Emmerthal, Germany, and, since 2005, the PV module and interconnection group. He currently develops characterization and production methods for photovoltaic modules.

Rolf Brendel studied in Freiburg and Heidelberg in Germany and with the University of Sussex, Sussex, U.K. He received the Physics Diploma degree in nuclear fusion research in 1987 and the Mathematics degree in 1988. In 1992, he received the Ph.D. degree in infrared spectroscopy from the University of Erlangen, Erlangen, Germany.

He then joined the Max Planck Institute for Solid State Research, Stuttgart, Germany, to study the physics of thin-film silicon solar cells and the thermodynamics of photovoltaic power conversion. In 1997, he became the Head of the Division for Thermosensorics and Photovoltaics, Bavarian Center for Applied Energy Research. In 2004, he joined the Institute of Solid State Physics, Leibniz University of Hannover, Hannover, Germany, as a Professor and became the Director of the Institute for Solar Energy Research in Hamelin (ISFH), Emmerthal, Germany. ISFH focuses research on crystalline Si photovoltaics. He has authored or coauthored a book and 230 research papers in this field.